6ICEGE 6th International Conference on Earthquake Geotechnical Engineering
1-4 November 2015
Christchurch. New Zealand

Bearing Capacity and Pull-Out Resistance of Wing Piles During Cyclic Vertical Loading

K. Urabe[1], K. Tokimatsu[2], H. Suzuki[3] and Y. Asaka[4]

ABSTRACT

This study tested one straight and four wing piles in a centrifuge to investigate the effects of shaft and wing diameter on bearing capacity and pull-out resistance during cyclic vertical loading. The results showed that before the shaft friction reached its ultimate value during cyclic loading, the pile tip resistance and the shaft friction were the main components resisting the vertical load. As a result, the shaft diameter controlled the response in the pushing direction and the shaft diameter and the wing ratio (the ratio of wing diameter to shaft diameter) controlled the response in the pulling direction. After the shaft friction reached its ultimate value, the pile tip resistance and the wing resistance were the main components resisting the vertical load. Therefore, the shaft and wing diameters controlled the response in the pushing direction and the wing ratio and wing area controlled the response in the pulling direction.

Introduction

During earthquakes, piles supporting structures suffer cyclic vertical loading due to the overturning moment from the structure. In the case of structures with high aspect ratios, the vertical load induced by the overturning moment can be large. Cyclic vertical loading reduces frictional resistance of piles, which also affects the bearing capacity and pull-out resistance. This decrease in frictional resistance may cause permanent tilt of a structure. However, the specific mechanism causing this phenomenon has not been thoroughly examined. Suzuki et al (2013, 2014) conducted vertical loading tests on wing piles (piles with a wing plate near the pile tip) with different wing diameters. This study investigated the influence of both the shaft and wing diameters of wing piles on bearing capacity and pull-out resistance during cyclic vertical loading.

Description of centrifuge model tests

This study conducted centrifuge model tests on one straight pile and four wing piles. The values in this part correspond to the values of the model scale and not the prototype scale. Figure 1 shows a generic test model. A single pile was set with an embedment depth of 250 mm in dry Toyoura sand (e_{max} = 0.982, e_{min} = 0.604) that was air-pluviated in a cylindrical rigid box with a relative density of 90~96 % and height of 400 mm. Figure 2 shows the five pile models and Table 1 lists their characteristics. Each pile had a different shaft diameter D and wing diameter D_w. Pile IDs are defined by shaft diameter, pile type and wing ratio D_w/D. The pile models were

[1]K. Urabe, Graduate student, Dept. of Architecture and Building Engineering, Tokyo Institute of Technology, Japan
[2]K. Tokimatsu, Professor, Dept. of Architecture and Building Engineering, Tokyo Institute of Technology, Japan
[3]H. Suzuki, Associate Professor, Dept. of Architecture and Civil Engineering, Chiba Institute of Technology, Japan
[4]Y. Asaka, Senior Research Engineer, Institute of technology, Shimizu Corporation, Japan

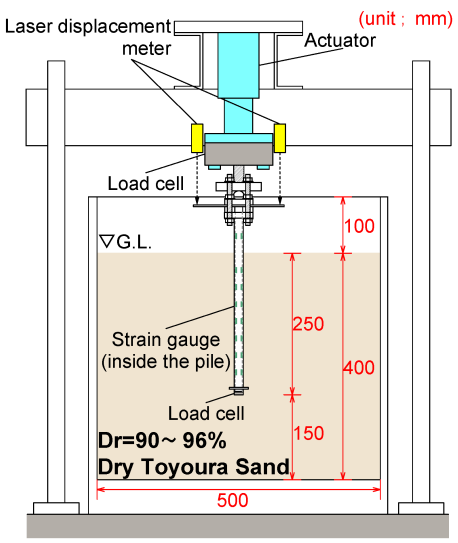

Figure 1. Test setup.

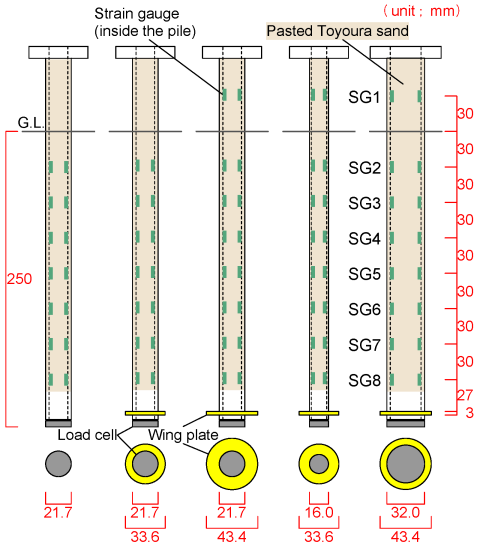

Figure 2. Pile models.

Table 1. Characteristics of pile models.

ID	Pile type	Shaft diameter D [mm]	Wing diameter D_w [mm]	Wing ratio D_w/D	Wing area A_w [$\times 10^2$mm^2]	Thickness of pile t [mm]
2S	Straight pile S	21.7	-	-	-	3.0
2W1.5	Wing pile W	21.7	33.6	1.5	5.2	3.0
2W2.0		21.7	43.4	2.0	11.1	3.0
1W2.1		16.0	33.6	2.1	6.9	1.5
3W1.4		32.0	43.4	1.4	6.8	3.0

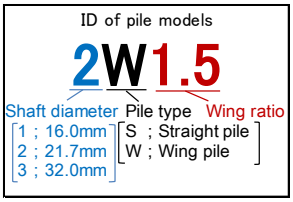

made of stainless steel pipes (JIS SS304) and Pile-2S had no wing plate. The other pile models had a wing plate made of stainless steel that was welded to the pipe near the tip. Each pile had strain gauges on the inner surface of the pipe at seven or eight depths and a load cell at the tip. To increase the shaft friction, dry Toyoura sand was pasted on the surface of each pile.

Displacement controlled monotonic and cyclic vertical loading tests were conducted with a loading rate of about 1.0 mm/min and centrifugal acceleration of 30G. Table 2 lists the tests performed and Figure 3 shows the loading histories. Figure 3(a) shows that, in the monotonic loading tests, the piles were pushed or pulled to the designated vertical displacement. Figure 3(b) shows that, in the cyclic loading tests, the loading displacement amplitude was gradually increased in four steps (±0.217, 1.09, 2.17 and 3.26 mm) repeated three times in each step. The four steps are 1, 5, 10 and 15 % of 21.7 mm, which is the shaft diameter of piles 2S, 2W1.5 and 2W2.0. In the tests, the vertical load and displacement at the pile head, the tip resistance, and the axial strains at seven or eight depths of the piles were recorded. Figure 4 shows the forces acting on a pile, which are defined by the following equations:

$$Q_c = R_p + R_{fc} \quad \text{< straight pile in compression >} \quad (1)$$

$$Q_t = R_{ft} \quad \text{< straight pile in tension>} \quad (2)$$

$$Q_c = R_p + R_{fc} + R_{wc} \quad \text{< wing pile in compression >} \quad (3)$$

$$Q_t = R_{ft} + R_{wt} \quad \text{< wing pile in tension >} \quad (4)$$

Table 2. Tests performed.

Case ID	Pile	Loading	Loading displacement*1
2S_Sc	2S	Monotonic compressive loading Sc	+21.7mm (+1.00D)
2W1.5_Sc	2W1.5		+33.6mm (+1.55D)
2W2.0_Sc	2W2.0		+17.5mm (+0.81D)*2
1W2.1_Sc	1W2.1		+33.6mm (+2.10D)
3W1.4_Sc	3W1.4		+16.5mm (+0.52D)*2
2S_St	2S	Monotonic tensile loading St	−21.7mm (−1.00D)
2W1.5_St	2W1.5		−5.0mm (−0.23D)
2W2.0_St	2W2.0		−21.7mm (−1.00D)
1W2.1_St	1W2.1		−16.0mm (−1.00D)
3W1.4_St	3W1.4		−16.0mm (−0.50D)
2S_Cyc	2S	Alternately cyclic vertical loading Cyc	±0.217mm ⇒±1.09mm ⇒±2.17mm ⇒±3.26mm repeated 3 times in each step
2W1.5_Cyc	2W1.5		
2W2.0_Cyc	2W2.0		
1W2.1_Cyc	1W2.1		
3W1.4_Cyc	3W1.4		

*1…+：Pushing direction、−：Pulling direction
*2…Loaded until the pile head axial force reached the maximam loading capacity of the actuator

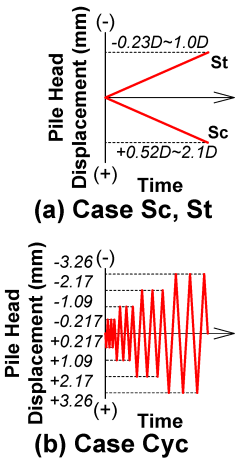

Figure 3. (a) Monotonic and (b) cyclic loading histories.

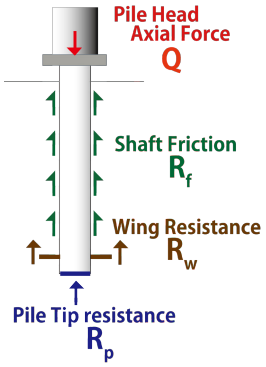

Figure 4. Forces acting on a pile.

where Q_c and Q_t are the pile head axial force, R_p is the tip resistance, R_{fc} and R_{ft} are the shaft friction, R_{wc} and R_{wt} are the wing resistance. The subscripts "*c*" and "*t*" indicate the values in compression (pushing) or tension (pulling), respectively. The shaft friction R_f is estimated from the difference between the pile head axial force Q and the axial force observed at strain gauges SG7. The wing resistance R_w is estimated from the difference between the axial force observed at strain gauges SG7 and the tip resistance R_p. In this study, positive values stand for compression and negative values stand for the tension. In addition, the subscripts "*s*" and "*c*" before the forces indicate the values in monotonic loading tests and the values in cyclic loading tests, respectively. The values in the following part correspond to the values of the prototype scale and not the model scale.

Effects of cyclic vertical loading on the tip resistance of piles

Figure 5 shows the relation of the pile head displacement with the tip resistance R_p. Solid lines and broken lines stand for the results of cyclic loading tests and monotonic loading tests, respectively. In the cyclic loading tests, the tip resistance R_p was larger than in the monotonic loading tests.

Figure 6 shows the relation of the loading step with the tip resistance in cyclic loading tests ${}_cR_p$.

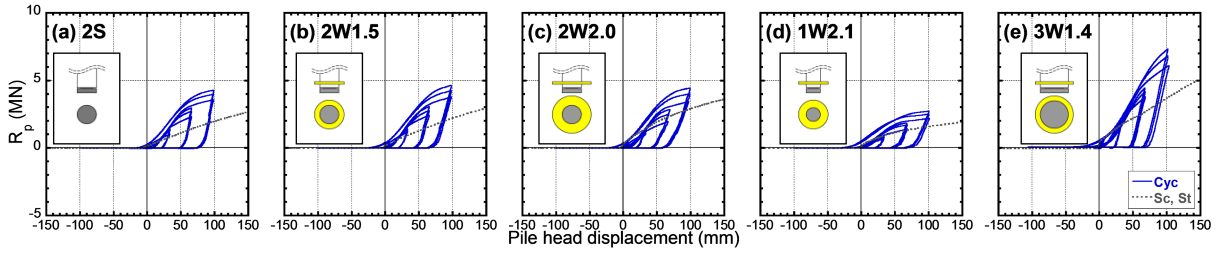

Figure 5. Relation of pile head displacement with tip resistance R_p.

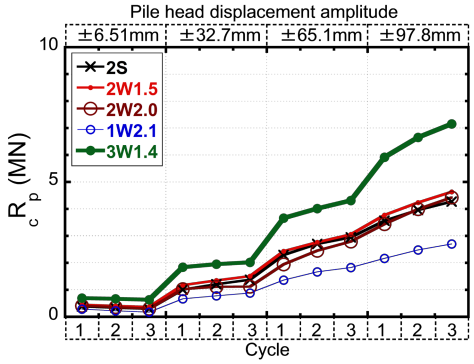

Figure 6. Relation of loading step with ${}_cR_p$.

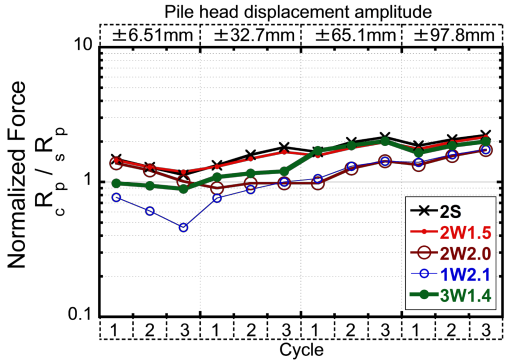

Figure 7. Relation of loading step with normalized tip resistance ${}_cR_p/{}_sR_p$.

As the pile head displacement amplitude and the number of cycles increased, the tip resistance ${}_cR_p$ increased. The tip resistance ${}_cR_p$ increased because the sand might have moved beneath the tip in tension and was densified by the tip in compression. This trend was more significant in the pile with a large shaft diameter (Pile-3W1.4) because a large amount of sand moved beneath the tip. To compare the results of cyclic loading tests to monotonic loading tests, the normalized tip resistance is computed as the ratio of the cyclic tip resistance ${}_cR_p$ to the monotonic tip resistance ${}_sR_p$ with the same displacement amplitude and cycle. Figure 7 shows the relations of the loading step with the normalized tip resistance ${}_cR_p/{}_sR_p$. Regardless of whether the pile had a wing or not and the size of the shaft and wing diameters, when the pile head displacement amplitude was about ±100 mm (10~20 % of the shaft diameter D), the normalized tip resistance ${}_cR_p/{}_sR_p$ increased to about 2.0.

Effects of cyclic vertical loading on the shaft friction of piles

Figure 8 shows the relations of the pile head displacement with the shaft friction R_f. During the monotonic loading tests the shaft friction R_f reached an ultimate value when the displacement was about ±30-100 mm (6~13 % of the shaft diameter D), and decreased gradually with increasing displacement. In contrast, during cyclic loading tests, the shaft friction R_f reached an ultimate value when the pile head displacement amplitude was about ±30 mm (3~6 % of the shaft diameter D), and decreased significantly with increasing displacement regardless of whether the pile had a wing or not and the size of the shaft and wing diameters.

Figures 9 and 10 show the relation of the loading step with the cyclic shaft friction in

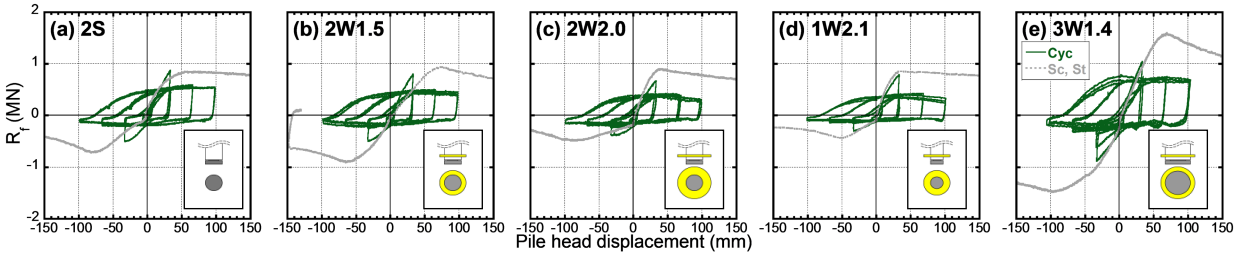

Figure 8. Relations of pile head displacement with shaft friction R_f.

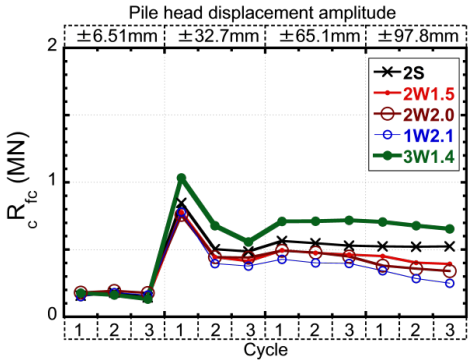

Figure 9. Relations of loading step with $_cR_{fc}$.

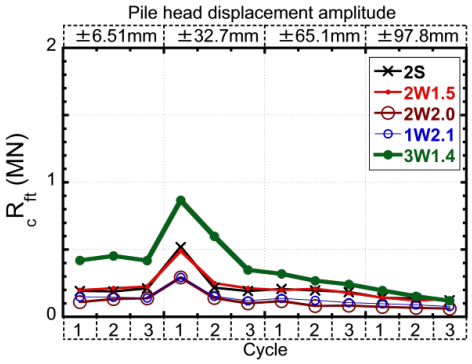

Figure 10. Relations of loading step with $_cR_{ft}$.

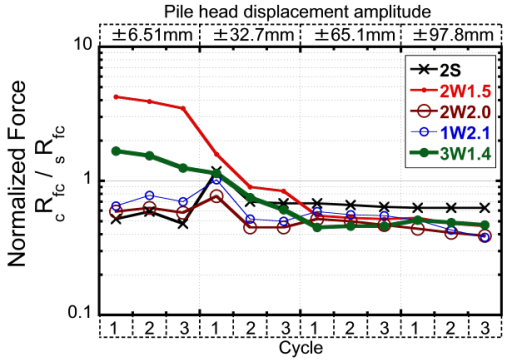

Figure 11. Relations of loading step with normalized shaft friction $_cR_{fc}/_sR_{fc}$.

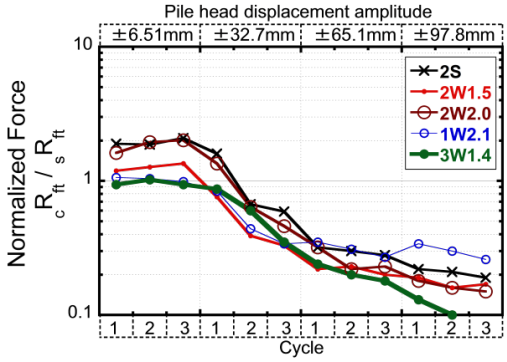

Figure 12. Relations of loading step with normalized shaft friction $_cR_{ft}/_sR_{ft}$.

compression $_cR_{fc}$, and the cyclic shaft friction in tension $_cR_{ft}$, respectively. The shaft friction in tension $_cR_{ft}$ decreased more than the shaft friction in compression $_cR_{fc}$. This is probably because the shear deformation caused by pushing the pile acted to increase the effective stress in the soil around the pile, whereas pulling the pile caused the effective stress around the pile to decrease. Figure 10 shows that the shaft friction $_cR_{ft}$ was smaller in Pile-2W2.0 and 1W2.1 than the others. This is probably because it has a larger wing ratio that lifted up more of the soil around the pile. Then, the vertical relative displacement between the soil and the pile decreased, which also decreased the shear deformation of the soil around the pile. Figures 11 and 12 show the relations of the loading step with the normalized shaft friction $_cR_{fc}/_sR_{fc}$ and $_cR_{ft}/_sR_{ft}$ respectively. Regardless of whether the pile had a wing or not and the size of the shaft and wing diameters, when the pile head displacement amplitude was about ±100 mm (10~20 % of the shaft diameter D), the normalized shaft friction $_cR_{fc}/_sR_{fc}$ reduced to about 0.5 and the normalized shaft friction $_cR_{ft}/_sR_{ft}$ reduced to about 0.2.

Effects of cyclic vertical loading on the wing resistance of piles

Figure 13 shows the relations of the pile head displacement with the wing resistance R_w. In the pushing direction of cyclic loading tests, the wing resistance R_w increased with increasing the loading steps. In contrast, in the pulling direction, the wing resistance R_w decreased with

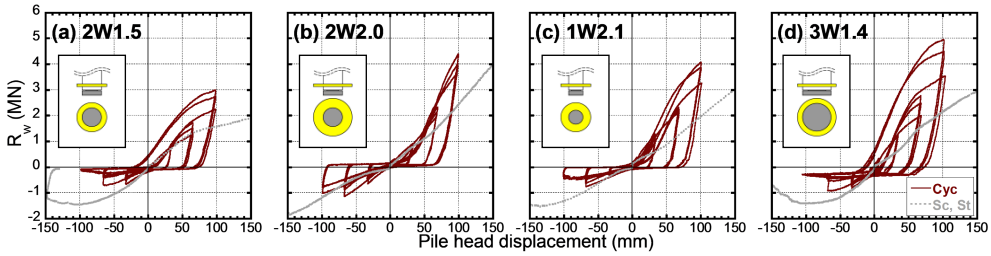

Figure 13. Relation of pile head displacement with wing resistance R_w.

increasing the loading steps, except Pile-2W2.0.

Figures 14 and 15 show the relation of the loading step with the wing resistance in cyclic loading tests ${}_cR_{wc}$ and ${}_cR_{wt}$ respectively. Figure 14 shows that the wing resistance ${}_cR_{wc}$ increased as both the pile head displacement amplitude and the number of cycles increased. Similar to the tip resistance ${}_cR_p$, the wing resistance ${}_cR_{wc}$ increased because sand might have moved beneath the wing during tension and densified during compression. In contrast, when the pile head displacement amplitude was more than ±65 mm, the wing resistance ${}_cR_{wt}$ in the wing piles with a small wing area (Pile-2W1.5, 1W2.1 and 3W1.4) decreased significantly, while the wing resistance ${}_cR_{wt}$ in the wing piles with a large wing area (Pile-2W2.0) did not show a significant

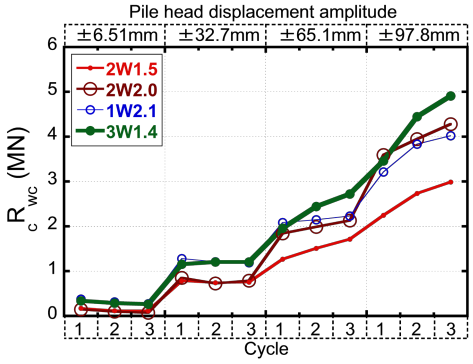

Figure 14. Relation of loading step with ${}_cR_{wc}$.

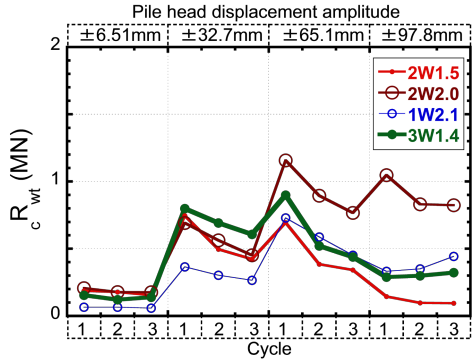

Figure 15. Relation of loading step with ${}_cR_{wt}$.

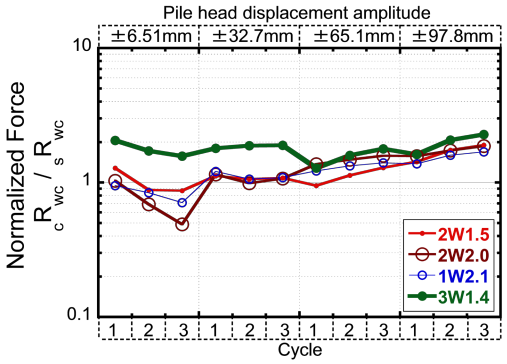

Figure 16. Relation of loading step with normalized wing resistance ${}_cR_{wc}/{}_sR_{wc}$.

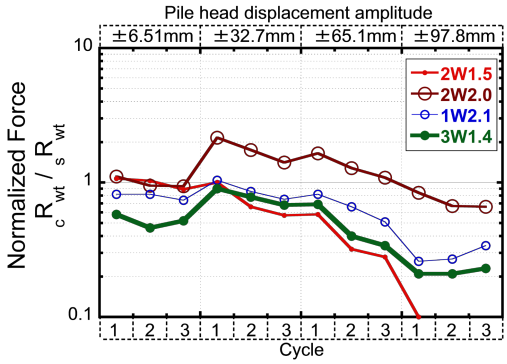

Figure 17. Relation of loading step with normalized wing resistance ${}_cR_{wt}/{}_sR_{wt}$.

decrease. This decrease was probably induced by a disturbance and a decrease of density of the soil above the wing. Figures 16 and 17 show the relation of the loading step with the normalized wing resistance ${}_cR_{wc}/{}_sR_{wc}$ and ${}_cR_{wt}/{}_sR_{wt}$ respectively. Figure 16 shows that, regardless of the size of the shaft and wing diameters, when the pile head displacement amplitude was about ±100 mm (10~20 % of the shaft diameter), the normalized wing resistance ${}_cR_{wc}/{}_sR_{wc}$ increased to around 2.0. In contrast, Figure 17 shows that when the pile head displacement amplitude was about ±100 mm (10~20 % of the shaft diameter), the normalized wing resistance ${}_cR_{wt}/{}_sR_{wt}$ in the wing piles with a small wing ratio D_w/D (Pile-2W1.5 and 3W1.4) reduced to 0.3, while the normalized wing resistance ${}_cR_{wt}/{}_sR_{wt}$ in the wing piles with a large wing ratio D_w/D (Pile-1W2.1 and 2W2.0) only decreased to about 0.3-0.7. This suggests that the decrease of the wing resistance during tension of cyclic loading might have been affected by both the wing ratio and the wing area.

Effects of cyclic vertical loading on the pile head axial force of piles

Figure 18 shows the relations of the pile head displacement and the pile head axial force *Q*. During compression of the cyclic loading tests, the pile head axial force *Q* increases as the pile head displacement amplitude and the number of cycles increases. In contrast, during tension, the pile head axial force *Q* decreases significantly as the pile head displacement amplitude and the number of cycles increases, except Pile-2W2.0.

Figure 19 shows the relations of the loading step with the pile head axial force in cyclic loading tests ${}_cQ_c$ and ${}_cQ_t$ respectively, which are the sum of the tip resistance ${}_cR_p$, the shaft friction ${}_cR_{fc}$ or ${}_cR_{ft}$ and the wing resistance ${}_cR_{wc}$ or ${}_cR_{wt}$. In the pushing direction (Figure 19(a)-(e)), when the pile head displacement was less than about ±30 mm, the pile tip resistance ${}_cR_p$ and the shaft friction ${}_cR_{fc}$ were the main components resisting the vertical load, so that the pile head axial force ${}_cQ_c$ in the pile with a large shaft diameter (Pile-3W1.4) was the biggest of that of the five piles. Thereafter, the pile tip resistance ${}_cR_p$ and wing resistance ${}_cR_{wc}$ were the main components resisting the vertical load, so that the pile head axial force ${}_cQ_c$ in the pile with a large shaft and wing diameters (Pile-3W1.4) was the biggest of that of the five piles. In contrast, in the pulling direction (Figure 19(f)-(j)), when the pile head displacement was less than about ±30 mm, the shaft friction ${}_cR_{ft}$ was the main component resisting the vertical load, so that the pile head axial force ${}_cQ_t$ in the pile with a large shaft diameter and small wing ratio (Pile-3W1.4) was the biggest of that of the five piles. Thereafter, the wing is the main component resisting the vertical load in the pulling direction, so that the pile head axial force ${}_cQ_t$ in the pile with a large wing ratio and wing area (Pile-2W2.0) was the biggest of that of the five piles.

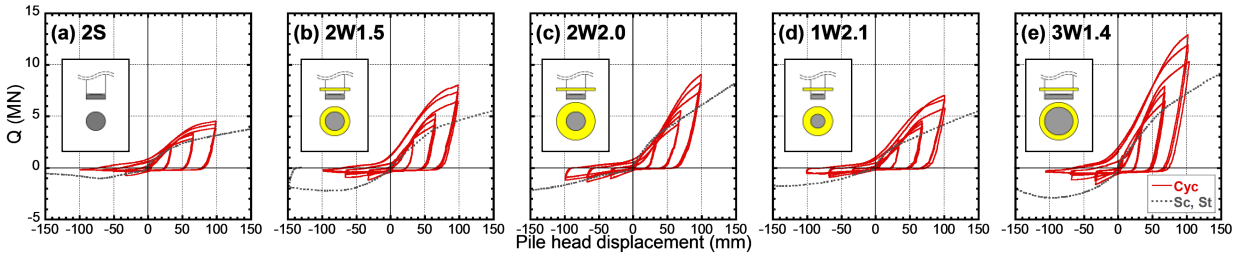

Figure 18. Relation of pile head displacement with pile head axial force *Q*.

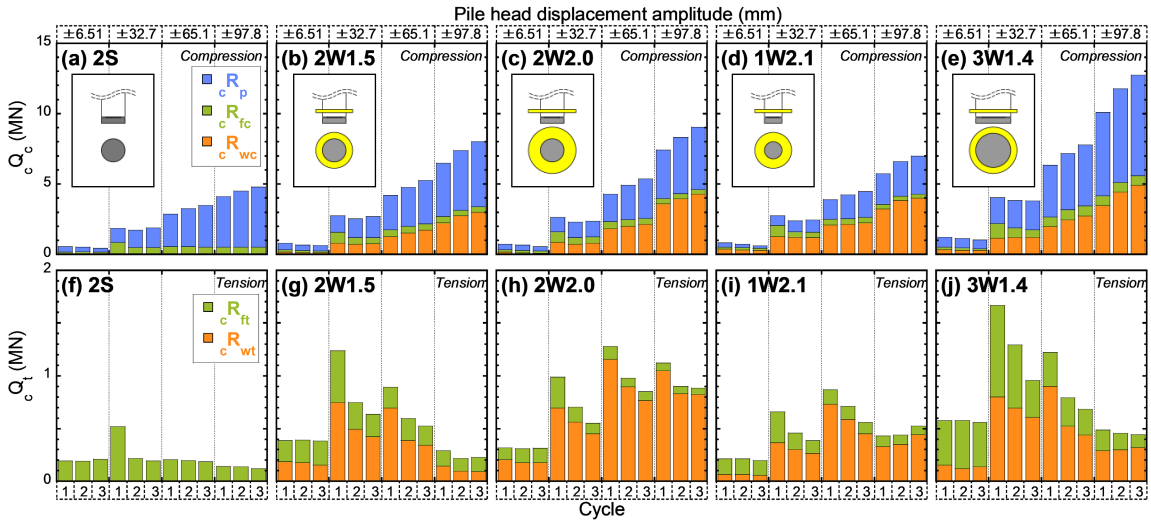

Figure 19. Relation of loading step with ${}_cQ_c$ and ${}_cQ_t$.

Conclusions

The result of the vertical loading tests on the straight and wing piles in the centrifuge led to the following conclusions:

1) Before the shaft friction reached its ultimate value during cyclic loading, the pile tip resistance and the shaft friction were the main components resisting the vertical load. Therefore, the shaft diameter controlled the response during compression whereas both the shaft diameter and the wing ratio controlled the response during tension. Thereafter, the pile tip resistance and the wing resistance were the main components resisting the vertical load. Therefore, the shaft and wing diameters controlled the response during compression whereas the wing ratio and the wing area controlled the response during tension.

2) Regardless of whether the pile had a wing or not, the shaft friction after reaching its ultimate value, decreased to about 50 % in compression and about only 20 % in tension with respect to the same values in monotonic loading.

3) Wing piles had high compression and tension resistances, the latter of which were about wing ratio times those of a straight pile with the same shaft diameter. The tensile resistance of wing piles with a wing ratio of about 1.5 decreased significantly with increasing cyclic vertical displacement after the shaft friction reached its ultimate value, but that of wing piles with a wing ration of about 2.0 did not decrease.

References

Suzuki H, Inamura K, Tokimatsu K, Wada M, Mano H. Estimation of bearing capacity and pull-out resistance of a pile with or without a wing plate in alternately cyclic loading based on centrifugal model tests. *Proceedings of the 10th International Conference on Urban Earthquake Engineering*, Tokyo Institute of Technology, Japan, 2013.

Suzuki H, Urabe K, Tokimatsu K, Asaka Y. Experimental investigation on pull-out resistance of a pile with a wing plate in alternately cyclic loading. *Proceedings of the 10th National Conference in Earthquake Engineering*, Earthquake Engineering Research Institute, Anchorage, AK, 2014.